Thermal Conductivity of Pyrolytic Graphite at Low Temperatures. I. Turbostratic Structures*

C. A. KLEIN AND M. G. HOLLAND
Raytheon Research Division, Waltham, Massachusetts
(Received 27 May 1964)

The thermal conductivity along (K_{II}) and across ($K_{\perp}$) the layer planes of 5 specimens of pyrolytic graphite (PG) in their as-deposited condition has been investigated at temperatures ranging from 1.7 to 300°K. In both directions the conductivity increases with deposition temperature; the $K_{II}/K_{\perp}$ ratio, however, remains close to 3 in the liquid-helium region and rises rapidly to about 125 at 300°K. In part, these anisotropies are presumed to reflect a situation in which only a fraction of the deposit permits regular heat flow perpendicular to the deposition surface. Above 100°K the thermal conductivity measured in this direction is almost temperature-independent ($K_{\perp}\approx 2\times 10^{-2}$ W cm^{-1}°K^{-1}), while below 20°K it is nearly proportional to $T^{2.3}$, in accordance with the lattice specific heat C_L. At these temperatures the thermal resistance arises from boundary scattering, and judging from x-ray evidence the phonon mean free path may be taken as isotropic. Turbostratic stacking affects the shearing elastic constant quite drastically; with $c_{44}=0.702\times 10^{10}$ dyn/cm^2 as suggested by Komatsu for lampblack-base graphite, a theoretical analysis confirms that below 4°K major contributors to $K_{\perp}$ are out-of-plane modes, and, therefore, $K_{\perp}$ should exhibit the same temperature dependence as C_L. By contrast, along layer planes the thermal conductance has an anomalous temperature dependence ($\propto T^{2.5}$ from about 10 to 80°K), which reflects mainly the dispersive nature of bond-bending vibrations in graphite. At still lower temperatures K_{II} involves electronic contributions K_E and can be expressed as a sum of two terms $AT+BT^n$, where $n\approx 2.6$ as predicted from a long-wavelength treatment of the "effective" phonon velocity, which shows that in-plane modes are seriously enhanced relative to the part they play in C_L. Plots of K_{II}/T versus T^{n-1} for $T\lesssim 4$°K yield straight lines with intercepts A and slopes B that correlate closely with the deposition temperature. The slopes are direct measures of the phonon mean free paths (600 to 1200 Å, which corresponds to the polygonal zones of the wrinkled-sheet structure), and illustrate the gradual improvement in preferred orientation as the deposition temperature covers the range 1700 to 2300°C. In conjunction with measurements of the electrical resistivity parallel to the deposition surface, the intercepts point to Lorenz numbers $K_{E}\rho_{II}/T$ of the order of 3 to 4×10^{-8} (V/°K)^2. Within the framework of a simple two-band-model description of graphite, there is strong evidence for a bipolar term in the electronic thermal conductivity of turbostratic PG, which indicates that these Lorenz numbers may not be inconsistent.

I. INTRODUCTION

A DETAILED investigation of heat-transport mechanisms in graphite has been prevented by the lack of sufficiently large single-crystal specimens. Though heat conduction in synthetic polycrystalline graphites has received much attention,[1] their study has been rather inconclusive, first because of the random distribution of the highly anisotropic graphite crystallites, and second because of the presence of binder material of an ill-defined nature. Moreover, the problem of investigating the thermal conductivity of graphite at very low temperatures is complicated by the fact that the measured values are exceedingly small and are strongly influenced by the degree of crystalline perfection. These various factors are probably responsible for the inconsistencies in the published literature.

In recent years, it was shown feasible to produce massive specimens of pyrolytic graphite (PG) through thermal decomposition of a carbon-bearing gas on a refractory substrate at temperatures of the order of 2000°C.[2] These pyrolytic deposits are polycrystalline, but they exhibit a high degree of preferred orientation. The basal planes of each crystallite consist of hexagonally arrayed carbon atoms, and these planes tend to align themselves parallel to the deposition surface. The individual crystallites assemble into polygonal zones or grains connected by tilt boundaries, thus giving rise to "wrinkled sheets," which are packed to *almost* theoretical density. To some extent, the preferred orientation transfers the intrinsic crystallite anisotropy to the bulk properties of PG. This material can, therefore, be used with advantage to investigate layer-plane as well as c-direction transport phenomena in graphite.

On the basis of morphological characteristics pyrolytic graphites fall into three main categories of increasing crystallographic perfection: turbostratic structures, ordered (or graphitized) structures, and near-ideal structures. As indicated by x-ray analysis, these structures may deviate from the single-crystal pattern in terms of interlayer spacing, crystallite size, and c-axis alignment. Low-temperature thermal-conductivity measurements reveal significant differences in the behavior of turbostratic, graphitized, and near-ideal PG specimens; it appears that the interlayer spacing, or in other words, the number of stacking faults, plays a decisive role in this regard. The present contribution will be devoted entirely to turbostratic structures, by which we mean graphites whose adjacent basal planes are randomly rotated with respect to one another and

* An initial account of this work was presented at the St. Louis meeting of The American Physical Society, on 25 March 1963 [C. A. Klein and M. G. Holland, Bull. Am. Phys. Soc. 8, 208 (1963)].

[1] For a comprehensive bibliography, see G. A. Slack, Phys. Rev. 127, 694 (1962).

[2] For an introduction to pyrolytic graphite and relevant references, see C. A. Klein, Rev. Mod. Phys. 34, 56 (1962).

thus do not display evidence of three-dimensional ordering. A unique feature of our experimental work is that the measurements were made on a series of specimens deposited under practically identical conditions at temperatures ranging from 1700 to 2300°C. Representative crystallite-size values for these materials are[3] $L_c = 200$ Å (crystallite height) and $L_a = 250$ Å (crystallite width), hence they have a ratio L_c/L_a of about 0.80, which is typical of carbon-black products.

An analysis of thermal conductivity mechanisms in PG requires a fair knowledge of the lattice dynamics in graphite. A great deal of work has been done on this problem, mainly in connection with investigations of the specific heat behavior at liquid-helium temperatures; in this regard the semicontinuum theory developed by Komatsu[4] appears to be most successful. Graphite is treated as a system of elastically coupled thin plates whose vibrations are postulated to be separable into three kinds of modes: (a) transverse in-plane vibrations, (b) longitudinal in-plane vibrations, and (c) out-of-plane or bending vibrations. An essential feature of Komatsu's model is that the shearing elastic constant c_{44} should be very sensitive to variations in the interlayer spacing,[5] and thus that significant changes in the specific heat could be expected for different types of graphites. Indeed, as early as 1955, DeSorbo[6] had reported that the heat capacity of graphite at low temperatures depends on the crystallite size. The specific heat values of the largest crystallite-size specimens (Canadian natural graphite) are the smallest, while those of lampblack-base specimens (grade SA-25 graphite) are much higher. With the advent of PG it has been clearly established that the general pattern of phonon behavior in graphite accords with its theoretical description by Komatsu. Unambiguous information on longitudinal and transverse acoustic modes propagating along the c direction of near-ideal specimens has been derived from slow-neutron scattering experiments[7]; and turbostratic PG deposits were found to have the largest heat capacity of all known graphite varieties.[8] It will be the primary object of this paper to analyze the results of low-temperature thermal-conductivity measurements on the basis of these observations, or more specificially, on the basis of c_{44} values that reflect the highly faulted layer stacking in turbostratic material.[9]

At this point we may recall that the low-temperature thermal conductivity of bonded graphites exhibits an anomalous behavior in that it varies more rapidly with temperature than the specific heat.[10–12] As it is improbable that the phonon mean free path is actually decreasing with decreasing temperature, this anomaly must either be due to crystallite contact-resistance effects or be related to some anisotropic feature of the graphite matrix. Both possibilities have been investigated. Hove and Smith,[13] for instance, attribute the phenomenon to the presence of nongraphitic carbon in the binder material of synthetic specimens. Klemens,[14] on the other hand, proposed an explanation on the hypothesis that, for transport, "longitudinal" phonon polarization modes, which are negligible as far as the specific heat is concerned, may become quite significant primarily as a consequence of the crystallite geometry if the width to height ratio is much larger than one. The former interpretation rests on the existence of a nongraphitic second phase, whereas the latter presumes an anisotropic scattering-path configuration. Magnetic susceptibility results[15] imply that there is little if any nongraphitic carbon in pyrolytic graphite. As was noted earlier, x-ray work indicates that parallel and perpendicular to the basal planes the crystallite dimensions of as-deposited specimens are roughly identical. It follows that the temperature dependence of the thermal conductivity of turbostratic PG ought to be of critical importance in elucidating fundamental aspects of graphite physics.

First we must examine the nature of the investigated specimens in more detail; the degree of preferred orientation and its variation with deposition temperature will be of major concern in the present context (Sec. II). Thermal conductivity data taken along and across the various deposits in the 1.7 to 300°K temperature range are presented in Sec. III. Electrical resistivity measurements will also be reported both for completeness and because it can be inferred from the Wiedemann-Franz ratio that, while above, say, 20°K the principal mechanism for heat transfer in graphite is by lattice waves, this may not be true at very low temperatures. We will consider the role of electronic transport in Sec. V and discuss the relevant Lorenz number in the light of a recent description[16] of the electron-band structure of turbostratic PG. Section IV is devoted to a theoretical evaluation of the lattice conductivity in the two principal crystallographic directions at temperatures below 20°K; these calcula-

[3] O. J. Guentert, J. Chem. Phys. **37**, 884 (1962).
[4] K. Komatsu and T. Nagamiya, J. Phys. Soc. Japan **6**, 438 (1961); K. Komatsu, *ibid.* **10**, 346 (1955); K. Komatsu, Phys. Chem. Solids **6**, 380 (1958).
[5] This was also suggested, independently, by Krumhansl [J. C. Bowman and J. A. Krumhansl, Phys. Chem. Solids **6**, 367 (1958)].
[6] W. DeSorbo, J. Chem. Phys. **23**, 1970 (1955); see also W. DeSorbo and G. E. Nichols, Phys. Chem. Solids **6**, 352 (1958).
[7] G. Dolling and B. N. Brockhouse, Phys. Rev. **128**, 1120 (1962).
[8] B. J. C. van der Hoeven and P. H. Keesom, Phys. Rev. **130**, 1318 (1963).
[9] In an oral comment subsequent to Slack's presentation at the 1962 March meeting of The American Physical Society [G. A. Slack, Bull. Am. Phys. Soc. **7**, 192 (1962)], one of the present authors (CAK) first pointed out that the use of "single-crystalline" elastic constants may not be relevant in dealing with pyrolytic graphites.
[10] R. Berman, Proc. Phys. Soc. (London) **A65**, 1029 (1952).
[11] W. W. Tyler and A. C. Wilson, Phys. Rev. **89**, 870 (1953).
[12] A. W. Smith and N. S. Rasor, Phys. Rev. **104**, 885 (1956).
[13] J. E. Hove and A. W. Smith, Phys. Rev. **104**, 892 (1956).
[14] P. G. Klemens, Australian J. Phys. **6**, 405 (1953).
[15] D. B. Fischbach, in *Proceedings of the Fifth Conference on Carbon*, edited by S. Mrozowski, M. L. Studebaker, and P. L. Walker (Pergamon Press Inc., New York, 1963), Vol. 2, p. 27.
[16] C. A. Klein, J. Appl. Phys. **33**, 3338 (1962).

tions will be performed within the framework of Komatsu's[4] semicontinuum treatment of graphite. We conclude (Sec. VI) that the temperature dependence anomaly must be associated with idiosyncrasies in the phonon-velocity behavior, and that both electron- and phonon-transport processes in graphite are now well enough understood to explain the bulk of our results in a satisfactory manner.

II. MATERIALS AND PROCEDURE

Our measurements were made on five different specimens of pyrolytic graphite in their "as-deposited" condition. Four of these specimens (labeled RAY) were manufactured in Raytheon's Advanced Materials Department and are part of a set prepared specifically for the purpose of investigating the deposition-temperature factor as nearly independently of other process variables as possible; their basic characteristics are listed in Table I. In addition, we have made use of a product obtained from High Temperature Materials, Inc., which will be designated as HTM.

These materials were all deposited from methane on flat plates of commercial graphite at temperatures ranging from 1700 to 2300°C. The RAY series was produced in a resistance-heated furnace by injecting the carbon-bearing gas mixture at a rate of about 5 liter/min for 50 h, the deposition-chamber pressure being maintained at approximately 10 mm Hg.[17] The densities are as recorded in Table I; with increasing deposition temperature they approach the single-crystal density of 2.26 g/cm^3.

From (00l) reflections the interlayer spacing in as-deposited PG is found to lie between 3.42 and 3.43 Å, independently of the deposition temperature (see Table I). This implies a nearly complete lack of layer order (turbostratic stacking),[18] which is confirmed by the shape of the (hk) bands. The degree of preferred orientation, however, exhibits a pronounced

TABLE I. Structural characteristics of the investigated pyrolytic graphite specimens.

Specimen label	Deposition temperature (°C)	Density (g/cm^3)	Layer spacing (Å)	Preferred orientation[a] (deg)	Crystallite size (Å)
RAY-17	1700	2.13	3.42_8	28	180
RAY-19	1900	2.19	3.42_6	24	240
RAY-21	2100	2.20	3.42_2	22	270
RAY-23	2300	2.22	3.42_2	21	285
HTM	≈2100	2.19	3.42_8	22	···

[a] Half-width of the distribution at half-maximum intensity, in degrees.

[17] For a discussion of PG deposition techniques, see R. J. Diefendorf, J. Chim. Phys. 57, 815 (1960).

[18] For the sake of comparison we recall that the average c-axis lattice spacing of lampblack graphite is about 3.40 Å, which indicates that perhaps two-thirds of the adjacent basal planes are randomly rotated with respect to each other (see the reference cited in Ref. 5).

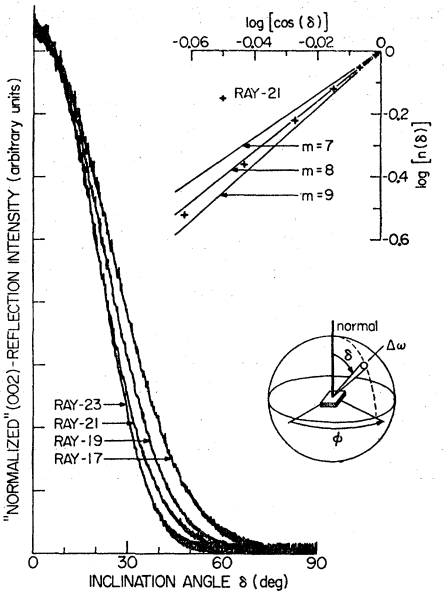

FIG. 1. Preferred orientation in pyrolytic graphite specimens deposited at temperatures ranging from 1700 to 2300°C (see Table I for particulars). The lower inset illustrates the concept of an orientation-density function $n(\delta)$ as defined in Sec. II. The RAY-21 distribution, which is typical of standard deposits, follows a $\cos^m\delta$ law with $m \approx 8$ (upper inset).

deposition-temperature dependence that warrants closer examination.

The preferred orientation of a PG deposit is best described in terms of an orientation-density function $n(\delta)$, which represents the relative number of crystallites whose c axis lies in a solid-angle element $\Delta\omega$ at δ degrees from the sample normal (see Fig. 1).[3] A measure of this "number" is the peak intensity of an (00l) reflection, when the diffraction vector points in the (δ,ϕ) direction. Since there is no azimuthal dependence the measurements can be made on thin cylindrical-rod samples cut parallel to the deposition surface, and $n(\delta)$ is then obtained by plotting the (002)-reflection intensity against the angle of rotation, after setting the diffractometer at the Bragg angle. The recordings shown in Fig. 1 illustrate an application of this procedure for the RAY series of turbostratic PG: There is a noticeable improvement in preferred orientation with increasing deposition temperature. The half-width of the distribution at half-maximum intensity (see Table I) provides a convenient quantitative description, because it corresponds, *grosso modo*, to the average misorientation angle of the basal planes with respect to the deposition surface. We may also note that, if we approximate the orientation densities by means of $\cos^m\delta$ functions, we find (see Fig. 1) that our 2100°C deposit has an "index" m of 8 in accordance with previous, more elaborate preferred-orientation studies.[19]

[19] O. J. Guentert and C. A. Klein, Appl. Phys. Letters 2, 125 (1963).

From x-ray line broadening measurements it appears that the average crystallite diameter L_a increases only from about 180 to 280 Å over the entire deposition-temperature range (see Table I).[20] As to the crystallite height, since our specimens are highly faulted its concept may have rather limited validity. However, if we equate the average dimension of coherently scattering regions across the layer planes to an L_c, it turns out that the crystallite-shape factor L_c/L_a is close to unity for most specimens of turbostratic PG. In this respect there is much similarity with the state of affairs in a graphitized lampblack, though the average crystallite size differs by a factor of more than two.

For the purpose of measuring the thermal conductivity and the electrical resistivity, rectangular rods were cut out of the various deposits in a "parallel" (along the layer planes) or a "perpendicular" (across the layer planes) geometry. Our measurements cover a temperature range extending from 1.7 to 300°K, and they were performed using the equipment and the procedure described by Holland and Rubin.[21] The two end faces of our samples were first copper plated, then soldered with pure indium to a heat sink and a heating element, respectively, prior to mounting in the high-vacuum chamber. The absolute temperature was monitored using carbon- or platinum-resistance thermometers, while the temperature gradient was measured with a gold-cobalt versus manganin thermocouple. With this arrangement the thermal conductivity is obtained from

$$K=(Q/A)(\Delta T/\Delta X)^{-1}, \qquad (1)$$

where Q is the power input from the heater, A the cross-sectional area, and $\Delta T/\Delta X$ the temperature gradient. Because of the very low thermal conductance of graphite at liquid-helium temperatures, heat losses may introduce serious errors; the use of exceptionally long lead wires, and in some cases replacement of copper lead wires by superconducting niobium wires, minimizes the problem. All factors considered our results are believed to be accurate within $\pm 3\%$ even for the lowest conductivity points.

III. EXPERIMENTAL RESULTS

Our thermal conductivity measurements for the set of specimens listed in Table I are summarized in Figs. 2 and 3. In both directions, parallel ($K_{\parallel}$) as well as perpendicular ($K_{\perp}$) to the deposition surface, the conductivity increases with deposition temperature. The $K_{\parallel}/K_{\perp}$ ratio, however, appears to be relatively insensitive to process parameters, which may lead us to conclude that the thermal anisotropy characteristic shown in Fig. 4 could be representative of the intrinsic anisotropy of graphite. In Sec. IIIA we demonstrate that this cannot be correct. The electrical resistivity was measured by a standard four-probe method; the data recorded in Fig. 5 extend previous work on turbostratic PG[16] to the liquid-helium region and show how $\rho_{\parallel}$ and $\rho_{\perp}$ behave when the temperature approaches absolute zero (Sec. IIIB). In Sec. IIIC we will then derive the two Wiedemann-Franz ratios from the curves in Figs. 2, 3, and 5, and discuss the implications in terms of phonon versus electron contributions to heat transport in pyrolytic graphite.

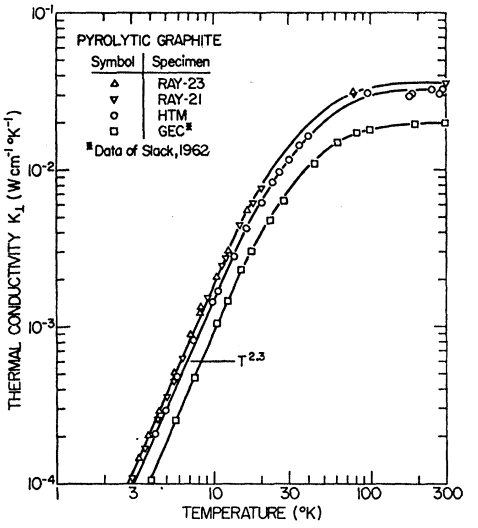

FIG. 2. Low-temperature thermal conductivity *across* the layer planes of turbostratic pyrolytic graphite. Specimens RAY-23, RAY-21, and HTM are described in Table I. Data referring to specimen GEC were taken from Fig. 1 in Phys. Rev. 127, 694 (1962); note that Slack's $K_{\parallel}$ corresponds to our $K_{\perp}$, and vice versa.

A. Thermal Conductivity

Across the layer planes, the low-temperature thermal conductivity of PG specimens deposited at 2100°C or higher is as shown in Fig. 2.[22] Above 100°K the conductivity is almost temperature independent ($K_{\perp}\approx 2\times 10^{-2}$ W units), while below 20°K it is nearly proportional to $T^{2.3}$. A similar behavior has been reported by Slack[23] for a piece deposited at 2250°C, though its conductivity is only about half of that obtained in our experiments. This observation confirms that significant variations in properties can be encountered with PG materials deposited at identical temperatures, primarily as a result of idiosyncrasies in the manufacturer's procedure.[24]

[20] It should be recognized that the "true" crystallite sizes might be slightly smaller than indicated in Table I, mainly because band-sharpening effects due to preferred orientation were not taken into account [O. J. Guentert (private communication)].

[21] M. G. Holland and L. G. Rubin, Rev. Sci. Instr. 33, 923 (1962).

[22] Serious difficulties were experienced in attempting to measure $K_{\perp}$ for 1700 and 1900°C material; they may be attributed to the presence of widespread thermal-resistance strips parallel to the deposition surface, which could prevent the attainment of a uniform heat-flow pattern across the layer planes of these "low-temperature" deposits (see also Ref. 29).

[23] Reference cited in Ref. 1.

[24] Slack indicates that his General Electric specimen was prepared at a total furnace pressure of 20 mm Hg, which is about twice the pressure used in the Raytheon process.

Along the layer planes, turbostratic PG exhibits a thermal conductivity that varies as a 2.5 power of temperature from about 10 to 80°K (see Fig. 3).[25] With Slack[23] we conclude that, contrary to statements by Smith and Rasor,[12] pyrolytic graphite does not have a basal-plane thermal conductance proportional to T^2, and thus cannot be cited as evidence for a "two-medium" explanation of the temperature-dependence anomaly (see Sec. I).[26] Furthermore, our data indicate that, over the whole deposition-temperature range, the temperature dependence of the thermal conductivity does not change—only the magnitude changes. This can be interpreted as reflecting variations in the phonon mean free path only[27] and is consistent with the x-ray results in Table I, which reveal a systematic improvement in crystallite size and preferred orientation with increasing deposition temperature. In this connection it is worth noting that our 2300°C deposit has a $K_{\parallel}$ of almost 5 W/(cm°K) at 300°K, or in other words, a room-temperature thermal conductivity greater than that of copper.

In Fig. 4 the measured thermal anisotropy ratio $K_{\parallel}/K_{\perp}$ is plotted against temperature. The ratio is close to 3 in the liquid-helium region but rises rapidly with temperature up to about 125 at 300°K, in contrast to the behavior of natural graphites whose thermal anisotropy apparently does not exceed 6.[1] It is often said that the enormous anisotropies of pyrolytic graphite, for heat as well as charge transport, reflect the highly preferred crystallite alignment in this material; we wish to emphasize that this is not so. Briefly, the argument goes as follows: In terms of the preferred-orientation index m introduced in Sec. II the *effective* (measured) anisotropy $K_{\parallel}/K_{\perp}$ of a homogeneous poreless system can be related to the *intrinsic* (crystallite) anisotropy K_a/K_c via[19]

$$\frac{K_{\parallel}}{K_{\perp}}=\frac{(m+2)K_a/K_c+1}{2K_a/K_c+(m+1)}. \tag{2}$$

For $m=8$,[28] the dependence is as illustrated in Fig. 4 (inset) and implies that $K_{\parallel}/K_{\perp}$ should not exceed 5. Hence, it is likely that the much greater anisotropy of pyrolytic graphite corresponds to a situation where only a fraction of the deposit is "organized" to permit a regular heat flow perpendicular to the deposition surface.[29] If the wrinkled sheets, for instance, are not in close contact over their whole surface, the measured c-direction conductivity will be less than the true conductivity of the crystallites, and there is no satisfactory means of circumventing this problem. With respect to the layer-plane conductivity we may write[19]

$$K_{\parallel}=K_a[1-(1-K_c/K_a)\langle\sin^2\delta\cos^2\phi\rangle], \tag{3}$$

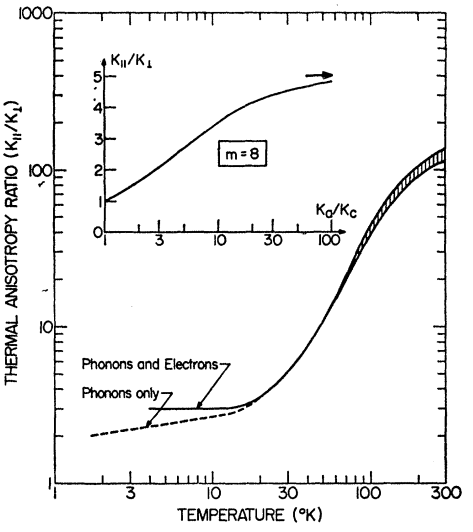

FIG. 4. Thermal anisotropy ratio as a function of temperature for specimens RAY-23, RAY-21, and HTM (see Table I). The "phonons only" characteristic refers to the layer-plane lattice components obtained in Figs. 14 and 15. The inset describes the relationship between effective and intrinsic anisotropy of a homogeneous graphite with a preferred-orientation index of 8.

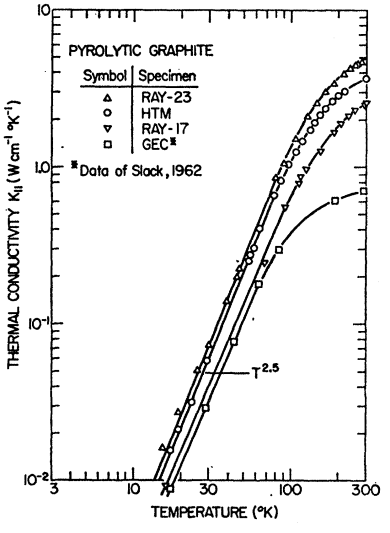

FIG. 3. Low-temperature thermal conductivity *along* the layer planes of turbostratic pyrolytic graphite. For the sake of clarity we have omitted plotting points for specimens RAY-21 and RAY-19. See also the caption of Fig. 2.

[25] Data taken at less than 10°K are recorded in Fig. 15.

[26] Subsequent heat treatment and graphitization do not alter this conclusion [M. G. Holland and C. A. Klein, Bull. Am. Phys. Soc. 7, 191 (1962)].

[27] J. C. Bowman, J. A. Krumhansl, and J. T. Meers, in *Industrial Carbon and Graphite* (Society of Chemical Industry, London, 1958), p. 52.

[28] This distribution is typical of 2100°C material and corresponds to an average angular tilt of 22° (see Fig. 1).

[29] Positive evidence for microcracks of about 500 to 2000 Å in length and presumably caused by a stress-induced separation of basal planes has recently become available through electron micrography [J. Pappis (private communication)].

where

$$\langle \sin^2\delta \cos^2\phi \rangle = \frac{1}{2}\left[\int_0^{\pi/2} n(\delta)\sin^3\delta d\delta\right] \times \left[\int_0^{\pi/2} n(\delta)\sin\delta d\delta\right]^{-1}, \quad (4)$$

which is simply $1/(m+3)$, as long as the $\cos^m\delta$ approximation of the orientation-density function holds.[30] For highly oriented deposits it follows that $K_{II} \approx K_a \times[(m+2)/(m+3)]$, if, as we may expect, heat conduction does not proceed preferentially across rather than along the tightly bound carbon-atom planes. Thus, we can probably consider the measured layer-plane thermal conductivity as an intrinsic basal-plane conductivity without injecting any serious error.

B. Electrical Resistivity

The results of electrical resistivity measurements along and across the layer planes of specimen HTM are recorded in Fig. 5, the probable error corresponding to the size of the points. These data are typical of turbostratic PG and supplement previously published work of this nature.[16] Even though the resistivity in the c direction is more than three orders of magnitude larger than along the layer planes, there is no significant difference in the temperature-dependence pattern. Both ρ_{II} and $\rho_{\perp}$ increase as the temperature is lowered, but below about 30°K they level off. Actually, both curves can be extrapolated to absolute-zero temperature almost horizontally, the layer-plane resistivity plateau

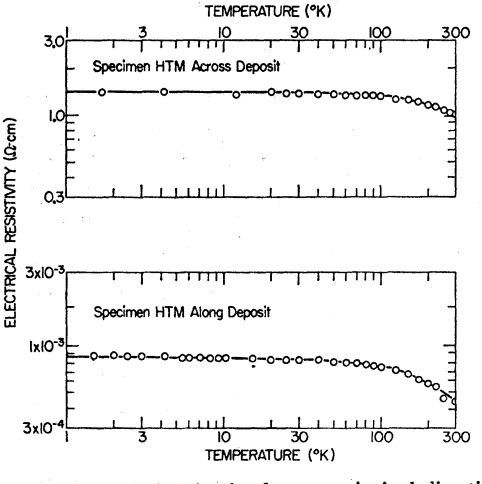

FIG. 5. Electrical resistivity in the two principal directions of turbostratic pyrolytic graphite at low temperatures. A logarithmic temperature scale was used in order to detect trends over the liquid-helium range. Note that, along as well as across the layer planes, the resistance becomes so insensitive to temperature that horizontal lines can be drawn through the experimental points.

[30] Note that, if we are dealing with a random distribution of crystallites ($m=0$), Eq. (3) yields $K=(2K_a+K_c)/3$, in accordance with standard practice.

occurring at exactly twice the room-temperature value ($\rho_{II}=440\ \mu\Omega$-cm). In this matter we have a close rapport with observations made on conventional graphites,[31] but that may be fortuitous because our measurements refer to turbostratic structures and cannot be fully interpreted within the framework of present electron-band models.[16]

C. Wiedemann-Franz Ratio

Thermal conductivity and electrical resistivity data taken across PG deposits combine to yield a Wiedemann-Franz ratio, $(K\rho/T)_{\perp}$, which is at least three orders of magnitude larger than the usual Lorenz

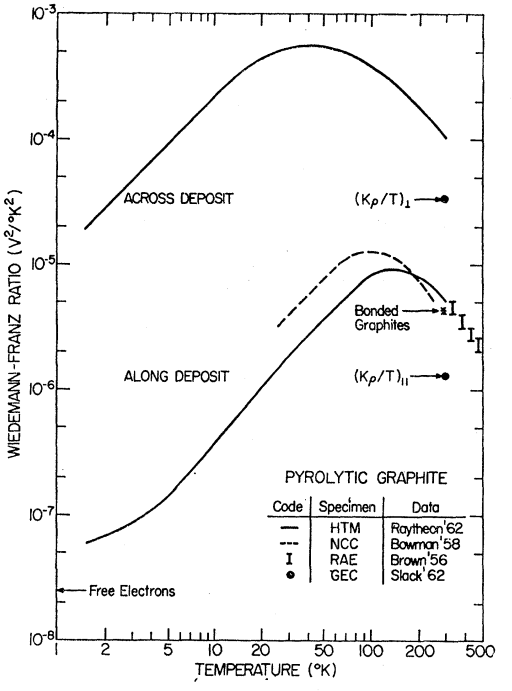

FIG. 6. Wiedemann-Franz ratio as a function of temperature. The two solid curves (parallel and perpendicular to the deposition surface) are representative of the pyrolytic graphite specimens listed in Table I. Note: HTM=High Temperature Materials, Inc.; NCC=National Carbon Company; RAE=Royal Aircraft Establishment; GEC=General Electric Company.

number (see Fig. 6). We conclude that, throughout the temperature range of interest, c-direction heat transport proceeds solely through the lattice. This statement does not apply to layer-plane transport. In Fig. 6 the $(K\rho/T)_{II}$ ratio is seen to be a strong function of temperature and to approach the "free-electron" value in the region below 4°K. In fact, if we estimate the electronic contribution to K_{II} on the basis of

$$K_E = \mathcal{L}_0 \sigma_{II} T, \quad (5)$$

with $\mathcal{L}_0=2.45\times10^{-8}$ (V/°K)^2, it turns out that trans-

[31] J. M. Reynolds, H. W. Hemstreet, and T. E. Leinhardt, Phys. Rev. **91**, 1152 (1953).

port by electrons may represent as much as 40% of the total heat conduction in the layer planes of turbostratic PG, at 2°K. Above about 10°K, the Wiedemann-Franz ratio $[(K\rho/T)_{11}=210\mathcal{L}_0$ at 300°K] implies that phonons predominate by far, in accordance with the usual interpretation of thermal conductance in graphite.[1] As shown in Fig. 6, near room temperature our layer-plane figure agrees with that of Brown *et al.*,[32] which is not surprising since their specimens were similar to ours. Quite unexpected, on the other hand, is that this seems to be the case also with pyrolytic filaments[33] and even with conventional graphites,[34] despite the fact that K and ρ vary by orders of magnitude. We may add that, in this light, Slack's[23] room-temperature results appear rather suspicious.

IV. PHONON PROCESSES

Around 2°K, lattice specific heat and c-direction thermal conductivity of turbostratic PG coincide in their temperature dependence ($\propto T^{2.3}$). As a first step we may, therefore, interpret $K_\perp$ in terms of the elementary theory of heat transport by lattice waves, the thermal resistance arising entirely from boundary scattering at crystallite interfaces (Sec. IVA). Along the layer planes, however, pyrolytic graphite appears to be "anomalous," and it will be shown in Sec. IVC that the reason for this probably lies in the character of the group velocities. Briefly, the phenomenon can be explained by considering the contributions originating from "in-plane" and from "out-of-plane" vibrations, the phonon-velocity configuration defining the "mix." These velocities depend on various elastic constants c_{ij}, and careful attention must be given to their numerical values. In this context we must also consider dispersion effects in the two principal directions of propagation in order to assess the range of validity of a long-wavelength treatment; this will be the main purpose of our investigation of lattice-dynamical features in turbostratic PG (Sec. IVB).

A. c-Direction Behavior

Thermal conductivity data taken perpendicular to the deposition surface at temperatures below 3°K are recorded in Fig. 7[35]: They obey a temperature-dependence law close to $T^{2.35}$, in good agreement with the indications of Fig. 2 for the range above 3°K. On the same figure we have also plotted the lattice specific heat of turbostratic PG as derived ($C_L=C-\gamma T$) from recent measurements by van der Hoeven and Keesom.[8] The confrontation indicates that, at least in the temperature range of experimental overlap, $K_\perp$ has almost the same temperature dependence as C_L, and thus that, in a first approximation, the c-direction thermal conductivity can be described according to the familiar equation for heat transport by phonons in a boundary-limited scattering situation, namely

$$K=(C_L v l)/3. \tag{6}$$

Here, the phonon velocity v and the phonon mean free path l are presumed independent of frequency, and C_L refers to the heat capacity per unit volume. On account of the discussion in Sec. IIIA regarding anisotropies in PG, it is reasonable to believe that the measured conductivity $K_\perp$ incorporates a "geometrical" reduction factor $1/z$. It follows that, on the basis of lattice specific heat and c-direction thermal conductivity measured at 2°K, the phonon mean free path across the layer planes of turbostratic material should be $0.98\ z/v$. Taking $v=3.45\times10^5$ cm/sec, which corresponds to longitudinal sound waves propagating in the c direction,[36] the mean free path is $280z$ [Å]; with $v=\frac{1}{3}(2V_t+V_l)$, or an average velocity of transverse and longitudinal waves, $l=575z$ [Å]. Moreover, it is not clear what value should be taken for z. Still, this simple analysis implies that the phonon mean free path might be determined primarily by scattering at grain boundaries rather than crystallite boundaries, since l appears to be greater than L_c, judging from x-ray indications (see Sec. II).[37]

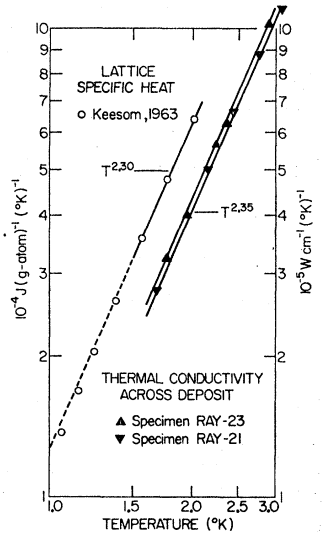

FIG. 7. A confrontation of lattice specific heat and c-direction thermal conductivity for turbostratic pyrolytic graphite at very low temperatures. The lattice specific heat is as calculated from data tabulated in Ref. 8. Note that the specific heat tends towards a T^3 dependence in the 1°K region.

[32] A. R. G. Brown, W. Watt, R. W. Powell, and R. P. Tye, Brit. J. Appl. Phys. **7**, 73 (1956).

[33] The NCC results in Fig. 6; they were taken from Ref. 27 and, presumably, refer to highly graphitic structures.

[34] At room temperature pitch-bonded stocks obey the following empirical relationship: $K\rho=3.1\times10^{-4}$ (Ω-cal)/(sec °K). [A. R. Ubbelohde and F. A. Lewis, *Graphite and its Crystal Compounds* (Oxford University Press, London, 1960), Chap. 3].

[35] Note that values of less than 3×10^{-5} W/(cm °K) were measured at around 1.7°K; in this temperature region these are lower values than those reported for any other known solid.

[36] E. P. Papadakis and H. Bernstein, J. Acoust. Soc. Am. **35**, 521 (1963).

[37] In essence, a similar conclusion was reached by Slack (reference cited in Ref. 1); in his calculation, however, Slack makes use of the heat capacities measured for large-crystallite-size natural graphites, which is inconsistent with the results of Ref. 8.

B. Lattice-Dynamical Considerations

In the Introduction we mentioned that a detailed description of lattice vibrational modes in graphite, at low temperatures, has been worked out by Komatsu.[4] For all practical purposes the normal modes separate into three frequency branches of the form

$$\nu_1^2 = v_l^2(\sigma_x^2+\sigma_y^2) + (\zeta/\pi^2 c_0^2)\sin^2(\pi c_0\sigma_z)\,, \tag{7a}$$

$$\nu_2^2 = v_t^2(\sigma_x^2+\sigma_y^2) + (\zeta/\pi^2 c_0^2)\sin^2(\pi c_0\sigma_z)\,, \tag{7b}$$

$$\nu_3^2 = 4\pi^2\kappa^2(\sigma_x^2+\sigma_y^2)^2 + (\mu^2/\pi^2)\sin^2(\pi c_0\sigma_z) + \zeta(\sigma_x^2+\sigma_y^2)\,, \tag{7c}$$

where $|\boldsymbol{\sigma}| = 1/\lambda$ is the phonon wave vector, $(\sigma_x^2+\sigma_y^2)^{1/2}$ its projection on the basal plane, and σ_z the hexagonal axis component; the parameters v_l, v_t, ζ, κ, and μ are as listed in Table II, and c_0 designates the interlayer spacing. Vibrations belonging to the ν_1 and ν_2 branches correspond to transverse and to longitudinal "in-plane" atomic displacements, respectively, while ν_3 vibrations lie nearly along the c axis for most propagation directions and hence are referred to as "out-of-plane" modes.

The last term in each of the Eqs. (7) originates from shearing interactions between neighboring layers. By fitting his theoretical specific-heat curve to DeSorbo's[6] data for Canadian natural graphite, Komatsu[4] deduced for the shearing elastic constant c_{44} a value of 4.05×10^{10} dyn/cm^2; from the compressibility normal to the layers he calculated $c_{33}=3.56\times10^{11}$ dyn/cm^2. An unambiguous confirmation of these estimates has been provided, recently, through Dolling and Brockhouse's[7] neutron-spectroscopy work using highly heat-treated near-ideal PG. With turbostratic material, however, we anticipate that layer disorder will affect the shearing elastic constant quite drastically and, to some extent, may also reduce the value of c_{33}. In our work all calculations were made taking the values suggested by Komatsu for lampblack-base graphite, namely $c_{33}=2.77\times10^{11}$ dyn/cm^2 and $c_{44}=0.702\times10^{10}$ dyn/cm^2. It has since become known that ultrasonic wave velocities in as-deposited PG[36] point to $c_{33}=2.58$ and $c_{44}=0.15$ in units of 10^{11} dyn/cm^2; bearing in mind that crystallite boundaries and crystallite misalignment may influence the measurements, we feel that these results are reasonably consistent with the corresponding values listed in Table II.

TABLE II. Numerical value and physical meaning of Komatsu's parameters (Ref. 4) for turbostratic graphite.

Symbol	Value	Meaning
v_l	2.10×10^6 cm/sec	velocity of in-plane longitudinal modes
v_t	1.23×10^6 cm/sec	velocity of in-plane transverse modes
κ	6.11×10^{-3} cm^2/sec	characterizes the layer-bending modulus
μ	1.06×10^{13} sec^{-1}	$\rho_0(\mu c_0)^2$: elastic constant c_{33}[a]
ζ	3.10×10^9 cm^2/sec^2	$\rho_0\zeta$: elastic constant c_{44}[a]

[a] ρ_0 is the volume density and c_0 the interlayer spacing; both are taken as in ideal graphite, i.e., 2.26 g/cm^3 and 3.35 Å, respectively.

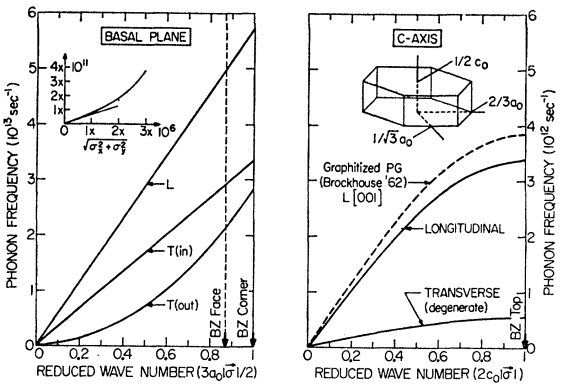

FIG. 8. Dispersion relations for acoustical phonons propagating along and across the basal planes of turbostratic graphite. These relations refer to Komatsu's (Ref. 4) semicontinuum treatment of lattice vibrations in lamellar structures. The L[001] dispersion curve for graphitized PG is as given by neutron spectroscopy (Ref. 7).

Figure 8 shows dispersion curves obtained on the basis of Eq. (7) after inserting elastic constants typical of turbostratic graphite. When traveling in the c-axis direction, out-of-plane modes are longitudinal and correspond to vibrations in which the carbon-atom sheets remain undistorted while the distance between layers is changing. The forces involved are purely interplanar, and the slope of the dispersion curve in the long-wavelength limit must, therefore, be determined by the elastic constant c_{33}.[38] For c-direction propagation the two in-plane branches are equivalent, and both are polarized perpendicular to the hexagonal axis. We note that, with a shearing elastic constant as indicated by Komatsu,[4] the frequency of these T[001] modes does not exceed 5.30×10^{11} sec^{-1}, even at the Brillouin-zone boundary [$|\boldsymbol{\sigma}| = 1/(2c_0)$]. Along the basal planes, however, the two in-plane branches split, and both become strong linear functions of the reduced wave number (see Fig. 8). They describe acoustical modes associated with stretching and shearing vibrations that propagate *within* aromatic carbon-atom sheets. Out-of-plane modes, on the other hand, involve bond-bending forces which render the dispersion non-Debye-like in a frequency range of interest to forthcoming developments (Sec. IVC). The inset on the left-hand side of Fig. 8 may help to clarify the picture in this respect.

Henceforth we restrict the discussion to wave vectors $\boldsymbol{\sigma}$ for which[39]

$$\sin^2(\pi c_0\sigma_z) \approx (\pi c_0\sigma_z)^2. \tag{8}$$

If θ designates the angle between phonon-propagation direction and crystallite c axis (see Fig. 9), the three frequency branches (7) may then be described as

[38] In this fashion Dolling and Brockhouse (Ref. 7) derived $c_{33}=(3.9\pm0.4)\times10^{11}$ dyn/cm^2 for near-ideal graphite.

[39] The approximation (8) requires $\sigma_z \lesssim 5\times10^6$ cm^{-1}.

follows:

$$\nu_1^2=\sigma^2[v_t^2\sin^2\theta+\zeta\cos^2\theta], \tag{9a}$$

$$\nu_2^2=\sigma^2[v_t^2\sin^2\theta+\zeta\cos^2\theta], \tag{9b}$$

$$\nu_3^2=\sigma^2[\zeta\sin^2\theta+(\mu c_0)^2\cos^2\theta+(4\pi^2\kappa^2\sin^4\theta)\sigma^2]. \tag{9c}$$

By referring to Table II we infer that shearing interactions between neighboring planes have relatively little effect, whereas bond-bending forces are of major significance in controlling the behavior of out-of-plane modes. At this point we may also consider the propagation velocities

$$v_1=(v_t^2\sin^2\theta+\zeta\cos^2\theta)^{1/2}, \tag{10a}$$

$$v_2=(v_t^2\sin^2\theta+\zeta\cos^2\theta)^{1/2}, \tag{10b}$$

$$v_3=\frac{\zeta\sin^2\theta+(\mu c_0)^2\cos^2\theta+2\sigma^2(4\pi^2\kappa^2\sin^4\theta)}{[\zeta\sin^2\theta+(\mu c_0)^2\cos^2\theta+\sigma^2(4\pi^2\kappa^2\sin^4\theta)]^{1/2}}, \tag{10c}$$

and investigate their anisotropy. This is best done in the long-wavelength limit, where the three vibrational branches become Debye-like. Figure 9 shows v_1, v_2, and v_3 plotted on a polar diagram and confirms that, perpendicular to the c axis, in-plane modes travel faster than out-of-plane modes, while along the c axis the situation is reversed.

C. Theoretical Evaluation

The thermal conductivity ellipsoid of graphite is a surface of revolution about the hexagonal axis (see inset in Fig. 9).[40] In the relaxation-time approximation

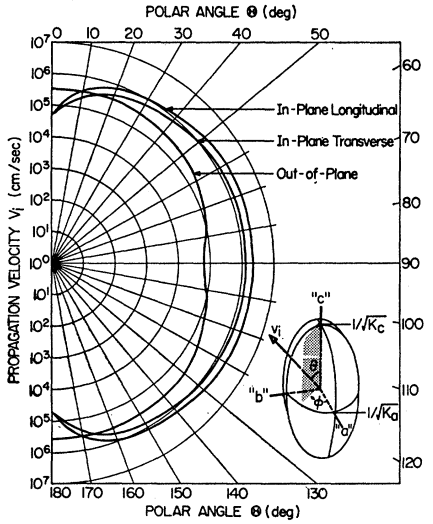

FIG. 9. Phonon-propagation velocities in turbostratic graphite (long-wavelength approximation). Note that, since graphite has an hexagonal crystal structure, these velocities are independent of the azimuthal angle ϕ. The inset illustrates the concept of a thermal conductivity ellipsoid for graphite.

[40] J. F. Nye, *Physical Properties of Crystals* (Oxford University Press, London, 1957), Chap. 11.

it can be shown that along principal directions (unit vector $\mathbf{s}$) of this ellipsoid the lattice thermal conductivity is[23]

$$K_S=\sum_i\int(\mathbf{v}_i\cdot\mathbf{s})^2\tau_iS_id^3\sigma. \tag{11}$$

Here, S_i, τ_i, and $\mathbf{v}_i$ represent heat capacity, relaxation time, and group velocity of the normal mode that belongs to the frequency branch i ($i=1$, 2, or 3) and has a wave vector $\boldsymbol{\sigma}$; the summation, of course, includes all the active phonon modes. In the temperature range under consideration the phonon mean free path is presumed to reflect boundary scattering only, so that we may take

$$\tau_i(\boldsymbol{\sigma})=l/v_i(\boldsymbol{\sigma}) \tag{12}$$

for all the modes. Furthermore, in the light of x-ray indications on crystallite size and crystallite shape (Sec. II), we assume that the phonon mean free path in turbostratic PG is virtually isotropic.[41] It follows that

$$K_c=l\sum_i\int v_i\cos^2\theta S_id^3\sigma, \tag{13a}$$

$$K_a=l\sum_i\int v_i\sin^2\theta\cos^2\phi S_id^3\sigma, \tag{13b}$$

if K_c refers to the conductivity in the direction of the hexagonal axis, and K_a to the conductivity along an arbitrary basal-plane direction. An evaluation of these integrals requires drastic approximations.[42] We propose to: (a) introduce "mean effective" velocities defined according to

$$\langle v_i\rangle_c=\frac{\int_0^\pi v_i\cos^2\theta\sin\theta d\theta}{\int_0^\pi\sin\theta d\theta}=\int_0^{\pi/2}v_i\cos^2\theta\sin\theta d\theta, \tag{14a}$$

$$\langle v_i\rangle_a=\frac{\int_0^\pi v_i\sin^3\theta d\theta\int_0^{2\pi}\cos^2\phi d\phi}{\int_0^\pi\sin\theta d\theta\int_0^{2\pi}d\phi}=\frac{1}{2}\int_0^{\pi/2}v_i\sin^3\theta d\theta; \tag{14b}$$

(b) evaluate these velocities in the long-wavelength limit; and (c) rewrite Eq. (13) in an approximate

[41] In this connection Klemens (Ref. 14) emphasizes that lattice waves are coupled together by "normal" three-phonon interactions, which tend to equalize the mean free paths.

[42] For a discussion of the procedure used in the case of isotropic solids, see P. Carruthers, Rev. Mod. Phys. 33, 92 (1961).

manner, namely

$$K_c = l\sum_i \langle v_i\rangle_c \int S_i d^3\sigma = l\sum_i \langle v_i\rangle_c C_i\,, \tag{15a}$$

$$K_a = l\sum_i \langle v_i\rangle_a \int S_i d^3\sigma = l\sum_i \langle v_i\rangle_a C_i\,. \tag{15b}$$

"In-plane" (C_1+C_2) and "out-of-plane" (C_3) contributions to the lattice specific heat of turbostratic graphite, at temperatures below 20°K, have been tabulated by Komatsu.[4] As to the mean effective velocities, in the long-wavelength limit they can be evaluated analytically (this is done in the Appendix), and the results are recorded in Table III. Though involving highly dispersive bond-bending vibrations, out-of-plane modes have velocities $\langle v_3\rangle_c$ and $\langle v_3\rangle_a$ that are almost frequency independent up to $|\sigma|\approx 3\times 10^6$ cm^{-1} and $|\sigma|\approx 1\times 10^6$ cm^{-1}, respectively; on this basis a rough approximation (using $h\nu = kT$) implies that, *in terms of our mean effective velocities*, a long-wavelength treatment might hold up to perhaps 20°K in the c direction, but not much above 4°K in the basal planes. In parenthesis we may point out that, for a situation characterized by an isotropic velocity configuration and a lack of polarization dependence, one has

$$\langle v_i\rangle_c = \langle v_i\rangle_a = v/3 \quad (i=1,\,2,\,3)\,, \tag{16}$$

which demonstrates that, in effect, Eq. (15) represents but a straightforward generalization of the "classical" case described by (6).

Taking $l=200$, 400, and 600 Å, Eq. (15a) yields K_c values as shown in Fig. 10. The calculation involves the effective phonon velocities $\langle v_i\rangle_c$ listed in Table III in conjunction with the specific heat components C_i derived by Komatsu[4] for lampblack-base graphite.[43] The plot shows that our method reproduces the temperature dependence of the thermal conductivity measured across PG deposits surprisingly well. Below 4°K the major contributors to K_c ($\approx 75\%$) are out-of-plane modes; since this is also the case with the specific heat,[44] both have a similar temperature dependence ($\propto T^{2.3}$). In the 10 to 20°K region, in-plane contributions may become quite substantial ($\approx 50\%$), but since the small shear interaction lowers their transition temperature[45] to below 10°K, they make no significant impact on the temperature dependence (see Fig. 10). As to the phonon mean free path, if we equate $K_\perp$ to K_c, Fig. 10 implies that $l\approx 400$ Å, which is about twice the crystallite size and not too different from the estimates in Sec. IVA, on the assumption of a reduction factor $1/z$ equal to one. Whatever the true situation in this regard, the confrontation of measured and calculated c-direction conductivities strongly suggests that, up to 20°K, the reduction factor operates in a frequency-independent manner.

TABLE III. "Mean effective" velocities of phonons in turbostratic graphite at very low temperatures [see Eq. (14) for a definition of $\langle v_i\rangle_c$ and $\langle v_i\rangle_a$, and Table II for indications regarding the various parameters].

Mean effective velocity	Analytical expression	Numerical value (10^5 cm/sec)
$\langle v_1\rangle_c$	$(\pi/16)v_t$[a]	2.41
$\langle v_2\rangle_c$	$(\pi/16)v_l$[a]	4.11
$\langle v_3\rangle_c$	$(\mu c_0/4)[1+\zeta/(\mu c_0)^2]$[b]	0.91
$\langle v_1\rangle_a$	$(3\pi/32)v_t$[a]	3.62
$\langle v_2\rangle_a$	$(3\pi/32)v_l$[a]	6.17
$\langle v_3\rangle_a$	$(\mu c_0/8)[1+(\zeta/\mu^2 c_0^2)\ln(4\mu^2 c_0^2/\zeta)]$[c]	0.50

[a] Note that shearing interactions between neighboring layers do not affect the mean effective velocities of in-plane modes.
[b] In the long-wavelength limit; numerical integrations show that $\langle v_3\rangle_c$ with v_3 as in Eq. (10c) varies by less than 10% for $0\leqslant|\sigma|\leqslant 3\times 10^6$ cm^{-1}.
[c] In the long-wavelength limit; numerical integrations show that $\langle v_3\rangle_a$ with v_3 as in Eq. (10c) varies by less than 10% for $0\leqslant|\sigma|\leqslant 1\times 10^6$ cm^{-1}.

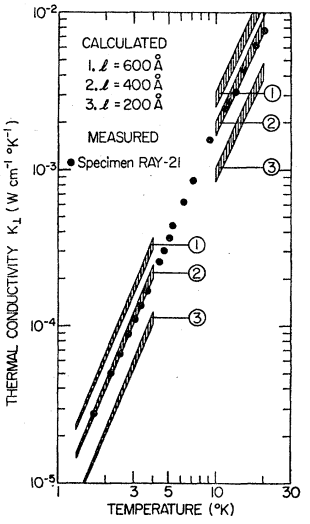

FIG. 10. Thermal conductivity measured perpendicular to the deposition surface ($K_\perp$) of turbostratic pyrolytic graphite in comparison with the c-axis conductivity (K_c) calculated for various scattering lengths. Note the slightly weaker temperature dependence above 10°K, which reflects the truncation of "in-plane" equal-frequency ellipsoids by the Brillouin-zone boundaries. The actual phonon mean free path is believed to be substantially greater than 400 Å, on account of textural features that may affect $K_\perp$.

In dealing with heat conduction along graphitic layer planes we cannot expect a simple equation such as (15b) to describe the state of affairs above, say, 4°K. At lower temperatures, a long-wavelength treatment indicates that, in a layer-plane direction, "in-plane"

[43] Since Komatsu's tabulation does not separate the two in-plane contributions, we have taken $K_c = l[(\pi/16)v(C_1+C_2)+(\mu c_0/4)\times(1+\zeta/\mu^2 c_0^2)C_3]$ with $v=v_t$ (upper values) and $v=v_l$ (lower values).

[44] The enhanced excitation of layer-bending vibrations induced by "relaxing" the elastic modulus c_{44}, which characterizes the lattice dynamics of randomly stacked lamellar structures, results in a noncubic heat capacity even at the lowest temperatures (for a detailed discussion, see the reference cited in Ref. 5).

[45] From a T^3 to a T^2 dependence, when constant-frequency contours commence intersecting with the upper and lower boundaries of the first Brillouin zone.

phonons travel on the average at least seven times faster than "out-of-plane" phonons. It follows that in-plane contributions to K_a will be seriously enhanced relative to the part they play in the lattice specific heat. Therefore, the temperature dependence of the basal-plane conductance (phonons only!) should be intermediate between that of C_1+C_2 and that of C_3 (see Fig. 11). As was mentioned earlier (Sec. IIIC), over the temperature range where $\langle v_3\rangle_a$ appears to be frequency independent, there is an appreciable electronic component, which prevents an unambiguous confirmation of the predicted lattice thermal-conductivity behavior. The problem will be re-examined in the next section; for the present we may rather consider the temperature-dependence anomaly above, say, 10°K. In this region the lattice dynamics is dominated by two phenomena: (a) The truncation in σ space,[45] which gives rise to quadratic in-plane contributions (they are Debye-like!). (b) The activation of out-of-plane modes with effective group velocities [in the sense of Eq. (14b)] that are roughly proportional to the wave vector. Indeed, the basal-plane thermal conductivity should be steeper than the specific heat, but in contrast to the situation at liquid-helium temperatures where in-plane modes play a critical role, above 10°K the temperature-dependence anomaly reflects mainly the dispersive nature of bond-bending vibrations in graphite.

Finally, if we refer to the dispersion curves in Fig. 8 and consider equivalent Debye temperatures (or simply the zone-boundary frequencies), it becomes apparent that the predominant wavelengths, at a given temperature, should be much greater in the layer planes than in the c direction. For this reason we expect crystal defects and other scatterers to be masked up to higher temperatures when transport occurs predominantly along rather than across the carbon-atom planes. The data in Figs. 2 and 3 fully support this line of reasoning.

V. ELECTRON PROCESSES

Figure 11 illustrates the predicted temperature dependence of the lattice thermal conductivity along the layer planes of turbostratic PG in the region below 4°K. We now wish to assess this calculation in the light of measurements presented, for instance, on the left side of Fig. 15. The conductivity falls much less rapidly than predicted; since it is unlikely that the phonon mean free path increases with decreasing temperature,[46] and recalling our previous discussion of the Wiedemann-Franz ratio (see Sec. IIIC), we are led to conclude that electrons are involved in layer-plane heat transport at very low temperatures. In Sec. VA we will analyze the data in a manner patterned upon the standard procedure used to evaluate phonon and electron contributions to the specific heat. In this connection we emphasize that,

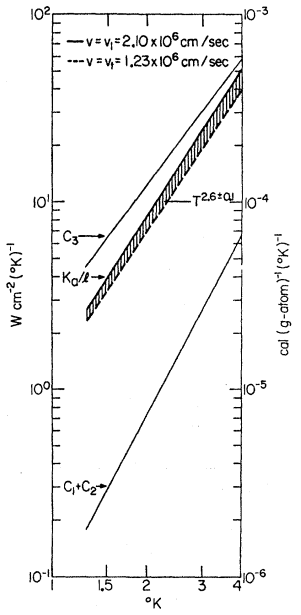

FIG. 11. Specific heat components per gram-atom and basal-plane thermal conductivity per unit length of a turbostratic graphite lattice at very low tenperatures. "In-plane" (C_1+C_2) and "out-of-plane" (C_3) heat capacities are as calculated by Komatsu (Ref. 4). Their combination according to $[(3\pi/32)\times v(C_1+C_2)+(\mu c_0/8)(1+\cdots)C_3]$, taking $v_t\leqslant v\leqslant v_l$, produces a lattice thermal conductivity that varies with temperature in a $T^{2.6\pm0.1}$-like manner.

because of the *semimetallic* character of graphite, the "usual" Lorenz number may not be adequate to describe the situation. In effect, the electronic contributions (Sec. VB) correspond to Lorenz numbers which exceed 2.45×10^{-8} (V/°K)^2, but it will be shown in Sec. VC that they are compatible with a two-dimensional approximation of the energy bands of graphite.

A. Layer-Plane Behavior

At very low temperatures we may attempt to express the thermal conductivity as a sum of two terms:

$$K_{11}=AT+BT^n, \tag{17}$$

where AT represents the electronic contribution (K_E) and BT^n the contribution due to the lattice (K_L).[47] The exponent n characterizes the temperature dependence of K_L and may, for the time being, be considered as a disposable parameter in the same manner as A and B. If the ansatz (17) is correct, experimental values of K_{11}/T, when plotted against T^{n-1}, should yield a straight line for $T\lesssim4$°K; a graphical analysis such as the one performed in Fig. 12 demonstrates that this is

[46] The c-direction behavior (see Sec. IV) is strong evidence against arguments of this sort.

[47] Note that electrons are presumed to have no effect on the mean free path of phonons in graphite; experimental (Ref. 12) and theoretical [J. E. Hove, North American Aviation, Inc., Technical Report No. NAA-SR-1398, 1956 (unpublished)] investigations of electron-phonon scattering in neutron-bombarded specimens have been quite conclusive in this regard.

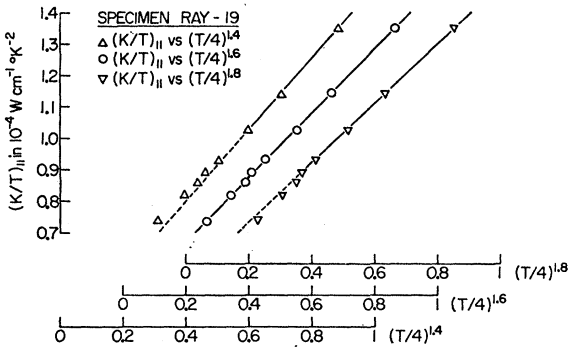

FIG. 12. Ratio of thermal conductivity and temperature measured parallel to the deposition surface of a pyrolytic graphite sample and plotted against various powers of the "reduced temperature" in the liquid-helium region. Specimen RAY-19 is described in Table I. It can be seen that the data fit an equation of the form $(K/T)_{\parallel}=A+B^*(T/4)^{1.6}$.

indeed the case with $n\approx 2.6$, which is precisely the type of lattice behavior predicted in the previous section.

In Fig. 13 we have replotted our low-temperature data for RAY and HTM material in the form $K_{\parallel}/T$ versus $T^{3/2}$.[48] The data fit the representation embodied in Eq. (17) remarkably well, especially considering the inherent difficulties of measuring the thermal conductivity at these low temperatures. Several features are to be noted:

(1) Each specimen generates a well-defined straight line with an intercept (A) and a slope (B) that correlate closely with the deposition temperature.[49] The slopes, in particular, show a striking dependency on the degree of lattice perfection. It appears that a plot of $K_{\parallel}/T$ versus $T^{3/2}$ at very low temperatures provides a most sensitive means of assessing structural characteristics of PG specimens.

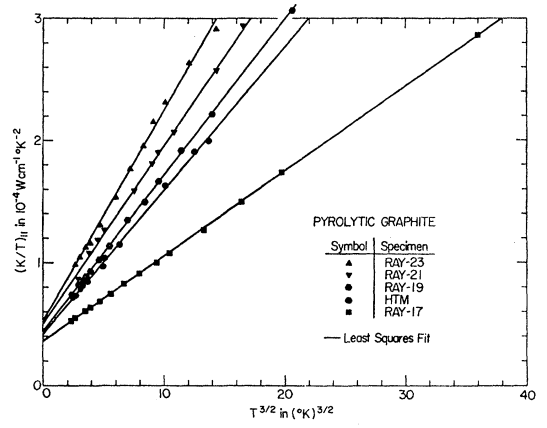

FIG. 13. Ratio of layer-plane thermal conductivity and temperature versus the temperature raised to the power $\frac{3}{2}$, for the set of pyrolytic graphites listed in Table I. The least-squares fits illustrate the validity of this representation and give a measure of phonon mean free paths and electronic heat conductivities. For particulars, see Table IV.

(2) The slopes in Fig. 13 are direct measures of the boundary-limited phonon mean free paths, and the values obtained in this way (by putting $B=l\sum_i\langle v_i\rangle_a \times C_i/T^{5/2}$) are listed in Table IV. These mean free paths are 3 to 5 times larger than the average crystallite diameters of Table I; on the other hand, they are similar in dimension to the polygonal zones observed by Kotlensky and Martens[50] in their electron-microscopic investigation of pyrolytic graphite. Since sharply delineated tilt boundaries delimit these zones, it could well be that small-angle "boundaries" between individual crystallites are rather ineffective in scattering long-wavelength phonons, which accords with the observation that, in its growth pattern, the mean free path follows more or less the improvement in preferred orientation (compare Figs. 1 and 13).

(3) The least-squares fits extrapolate to intercept values that vary from specimen to specimen. This is in order since the factor A of Eq. (17) relates to the electrical conductivity $\sigma_{\parallel}$. These intercepts determine the electronic contribution to the thermal conductivity, and they will be considered now in more detail.

B. Electronic Contribution

The nature of Eq. (17) permits a straightforward interpretation of the "zero-temperature" value of $K_{\parallel}/T$: If the Lorenz number is defined as $\mathfrak{L}\equiv K_E/(\sigma_{\parallel}T)$, then

$$A=\mathfrak{L}\sigma_{\parallel}. \tag{18}$$

Table IV includes $\mathfrak{L}$ numbers derived from the intercepts in Fig. 13 plus independent measurements of the electrical conductivity parallel to the deposition surface.[51] In comparison with the Lorenz number of metals these values are not very palatable; in the next section we will attempt to formulate the problem in a rigorous manner and see whether a quantitative analysis might yield a reasonable explanation.

Figures 14 and 15 illustrate how $K_{\parallel}$ divides into phonon and electron components. In turbostratic PG electronic contributions predominate below about 2°K, which explains the trend towards a $1/T$-type dependence shown by the thermal conductance in this temperature region. We may also note that, in magnitude, these contributions increase with deposition temperature in a manner quite analogous to the lattice behavior; once again we observe a strong mutual dependency of

[48] While Fig. 12 points to $n=2.6$, in general the data are also compatible with a $T^{2.5}$ dependence, which, of course, has the advantage of following the trend exhibited by the thermal conductivity in the pure-phonon range ($T>10$°K).

[49] Specimen HTM does not conform to the RAY pattern; the departure reflects variations in the manufacturing process.

[50] W. V. Kotlensky and H. E. Martens, Jet Propulsion Laboratory, Technical Report No. 32-360, 1962 (unpublished).

[51] The reader is reminded that $\sigma_{\parallel}$ remains constant over the whole temperature range of interest (see Fig. 5); however, because we had to use different samples for the electrical and the thermal measurements, the accuracy of the Lorenz numbers may not be better than 10%.

TABLE IV. Some results concerning layer-plane transport phenomena in turbostratic pyrolytic graphite (the specimens are described in Table I).

Specimen label	Slope[a] (10^{-5} W cm^{-1} °K$^{-7/2}$)	K_L at 2°K[b] (10^{-5} W cm^{-1} °K^{-1})	Phonon mean free path (Å)	Intercept[a] (10^{-5} W cm^{-1} °K^{-2})	$\sigma_{\parallel}$ at 2°K[c] (10^{3} Ω^{-1} cm^{-1})	$\mathcal{L}$ number (10^{-8} V^2 °K^{-2})
RAY-17	0.69	3.91	520	3.60	1.07	3.37
RAY-19	1.28	7.25	970	4.40	1.20	3.65
RAY-21	1.45	8.21	1100	5.09	1.26	4.05
RAY-23	1.73	9.80	1300	5.24	1.35	3.85
HTM	1.17	6.63	880	4.24	1.19	3.53

[a] Refers to the $K_{\parallel}/T = A + BT^{3/2}$ representation of low-temperature thermal conductivity data (see Fig. 13).
[b] Lattice thermal conductivity as derived from the $K_{\parallel}/T$ slope.
[c] Electrical conductivity measured parallel to the deposition surface.

phonon- and electron-transport mechanisms on structure and texture of PG deposits.

C. Lorenz Number

A great deal of attention has been given to the band structure of perfect graphite[52]; it will suffice to mention here that the small interaction between second nearest planes in an *abab* stacking arrangement gives rise to a certain amount of band overlap (E_0) at the Fermi energy. Transport takes place simultaneously in the valence and the conduction band, and the carriers must be treated by means of exact Fermi-Dirac statistics. Within the framework of a "simple two-band model" description of pyrolytic graphite[53] the electronic thermal conductivity must, therefore, be expressed as follows[54]:

$$K_E = T\left(\frac{k}{e}\right)^2\left[\gamma_h\sigma_h+\gamma_e\sigma_e+\frac{\sigma_h\sigma_e}{\sigma_h+\sigma_e}\left(\delta_h+\delta_e-\frac{E_0}{kT}\right)^2\right]. \quad (19)$$

Here, the subscripts h and e refer to holes and electrons, respectively, γ and δ are functions of the degree of degeneracy and the scattering mechanism, and $\sigma_{h,e}$ denotes the electrical conductivity of a single band. The first two terms on the right side of (19) represent the normal contributions due to holes and electrons, while the third term concerns the additional effect induced by bipolar diffusion. In this connection it should be noted that, even with E_0/kT appreciably larger than one, there can be a significant bipolar contribution, which may lead to a Lorenz number greater than the usual $\mathcal{L}_0 = (\pi^2/3)(k/e)^2$ of fully degenerate systems.

At this time, there is little information available on band structure or carrier scattering in turbostratic PG at very low temperatures. We may discuss the case, tentatively, by assuming that: (a) there is no band overlap,[55] (b) the mobility ratio is one,[56] and (c) the

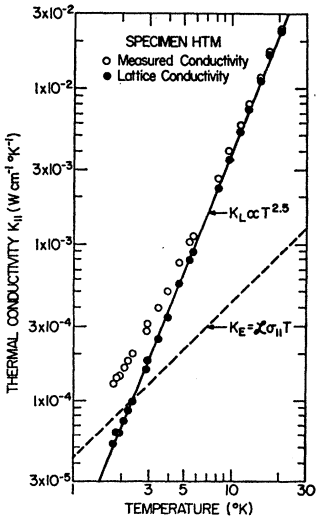

FIG. 14. Measured thermal conductivity ($K_{\parallel}$), lattice thermal conductivity (K_L), and electronic thermal conductivity (K_E) along the layer planes of turbostratic pyrolytic graphite. Specimen HTM is described in Table I. The electronic contribution was taken as indicated by the relevant intercept in Fig. 13.

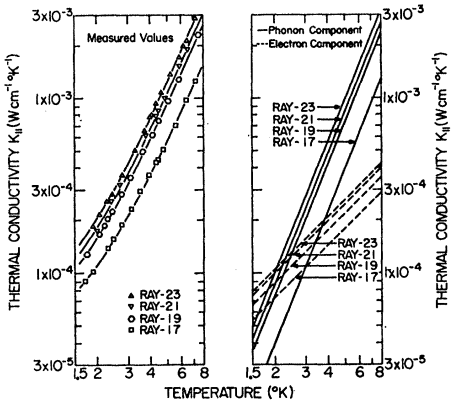

FIG. 15. Measured thermal conductivity and its phonon and electron components at very low temperatures for a series of pyrolytic graphite specimens deposited at 1700, 1900, 2100, and 2300°C. Structural characteristics of these specimens are summarized in Table I. The systematic dependence on deposition temperature appears to reflect the pattern exhibited by the degree of preferred orientation as illustrated in Fig. 1; this is also in accordance with the magnetoresistivity behavior reported in Ref. 16.

[52] For a state-of-the art review, see J. W. McClure, IBM J. Res. Develop. 8, 255 (1964).
[53] C. A. Klein, J. Appl. Phys. (to be published).
[54] C. F. Gallo, R. C. Miller, P. H. Sutter, and R. W. Ure, J. Appl. Phys. 33, 3144 (1962).
[55] Stacking faults are presumed to affect the interaction between second nearest carbon-atom planes and, thus, to reduce or even eliminate the overlap of upper and lower π bands; the relatively small coefficient of the linear term in the specific heat of as-deposited PG (see Ref. 8) appears to substantiate this point of view.
[56] Soule's work [D. E. Soule, Phys. Rev. 112, 698 (1958)] indicates that $\mu_e/\mu_h \approx 0.8$ in single-crystalline graphite at helium temperatures; with regard to turbostratic structures we have no independent element of judgement.

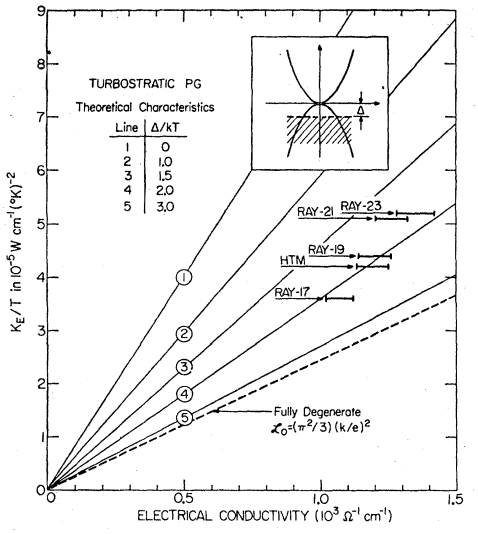

FIG. 16. Ratio of electronic thermal conductivity and temperature plotted against the electrical conductivity in the layer-plane direction. The slopes are indicative of the Lorenz numbers associated with various reduced Fermi energies, on the assumption of an energy-independent relaxation mechanism and a band-structure configuration as illustrated in inset. Experimental results point to substantial bipolar contributions in turbostratic pyrolytic graphite.

relaxation time is energy independent.[57] These are fairly reasonable assumptions; in any event, at this point it does not seem fruitful to speculate on possible "deviations" from this scheme. On these premises the Lorenz number becomes[53]

$$\mathcal{L}=(k/e)^2[a\gamma_0^+/(1+a)+\gamma_0^-/(1+a) +a(\delta_0^+ +\delta_0^-)^2/(1+a)^2]. \quad (20)$$

Equation (20) involves the carrier-density ratio $a=n_h/n_e$ and the functions

$$\delta_0^{\pm}=[5F_{3/2}(\pm\Delta/kT)][3F_{1/2}(\pm\Delta/kT)]^{-1}, \quad (21a)$$

$$\gamma_0^{\pm}=[7F_{5/2}(\pm\Delta/kT)][3F_{1/2}(\pm\Delta/kT)]^{-1} -(\delta_0^{\pm})^2, \quad (21b)$$

where F_j designates the Fermi-Dirac integral of order j, and Δ the depression of the Fermi level that accompanies electron trapping at internal defects and crystallite boundaries of turbostratic material. As to the carrier-density ratio, on the basis of work discussed elsewhere[16] we may write:

$$a=\ln[1+\exp(\Delta/kT)]/\ln[1+\exp(-\Delta/kT)]. \quad (22)$$

Plotted in Fig. 16 are K_E/T versus σ_{11} characteristics that correspond to Lorenz numbers obtained from (20) by taking $\Delta/kT=0$, 1, 1.5, 2, 3, and $\gg 1$ (fully degenerate). On the same plot are K_E/T values derived from our experiments: The confrontation yields strong evidence for bipolar contributions to the electronic thermal conductivity of turbostratic PG. Though it is clear that a more refined treatment will be required, the present approach demonstrates that Lorenz numbers such as those listed in Table IV warrant serious discussion and are not inconsistent with current energy-band models.

VI. CONCLUSION

In this paper we have been concerned with the low-temperature thermal conductivity of turbostratic pyrolytic graphites. Over the investigated temperature range, c-direction heat transfer proceeds entirely through the lattice. Along the layer planes, however, charge carriers are also involved and may even predominate at temperatures less than 2°K. The over-all behavior of both phonon and electron contributions can be understood, at least qualitatively, within the framework of theoretical models, if account is taken of the special features arising from the anisotropic as well as from the semimetallic character of graphite. Of course, our calculations are quite approximate and need refinement, especially with regard to dispersion effects and band configuration. Still, the agreement with experimental data is sufficiently good to lend a great deal of confidence in the basic picture developed in Secs. IV and V.

A major problem arises in connection with the thermal anisotropy since the measured ratio $K_{11}/K_{\perp}$ is inconsistent with the degree of preferred orientation of PG structures. In view of the microcrack situation the difficulty may well stem from a "geometrical" reduction factor that affects c-direction transport processes. For the thermal conductivity this factor could be of the order of 2 or 3 in the liquid-helium region and should be frequency independent. The sharp increase in the anisotropy as the temperature approaches 300°K might then be attributed, in part, to the onset of a frequency dependence, but convincing evidence must await the availability of less-faulted material. Lack of reliable information on the *magnitude* of c-direction transport seriously limits efforts to develop a truly satisfactory theoretical treatment of lattice conduction in PG. There is, really, little point in attempting to reformulate the problem in a more precise manner than was done here, considering the present uncertain experimental position.

Our discussion of lattice conduction in turbostratic PG reflects the essential fact that random stacking of adjacent basal planes leads to unusually small values of the shear modulus c_{44}. According to Komatsu's[4] theory of normal modes in graphite, by "relaxing" c_{44} one allows bond-bending vibrations of the basal planes to be excited at the lowest temperatures ($T\gtrsim 1.0$°K), and thus to inject dispersive elements even though the equal-frequency contours are still far from the Brillouin-zone boundaries. We believe that the unique features of

[57] At very low temperatures the electrical resistivity of turbostratic PG exhibits "flat" characteristics (see Fig. 5), which points to boundary-limited mean free paths; in Ref. 16 it is argued that this situation is consistent with a scattering parameter $s=0$.

thermal-energy transfer in turbostratic graphite can be identified with this and other aspects of the lattice vibrational spectrum illustrated in Fig. 8. In summary:

(1) Calculations based on Komatsu's semicontinuum treatment of graphite yield the correct temperature dependence of the thermal conductivity measured across PG deposits. Below 4°K the major contributors are out-of-plane modes, and since this is also the case with the specific heat, both exhibit a similar temperature dependence ($\propto T^{2.35}$).[58] Thus we may relate the c-direction behavior to the nature of the layer-bond bending forces that govern out-of-plane vibrations when the elastic limit ($4\pi^2\kappa^2\sigma^2 \ll \zeta$) is no longer appropriate.

(2) Up to almost 80°K, the lattice thermal conductivity of randomly stacked layer planes varies approximately as a 2.5 power of temperature, and hence, appreciably faster than the specific heat. At liquid-helium temperatures the explanation for this discrepancy lies in the long-wavelength phonon-velocity pattern, which enhances the relative contribution of Debye-like in-plane modes in comparison to the part they play in c-axis transport. Above about 10°K, when truncation occurs, the anomalous temperature dependence of K_{II} must be attributed to the gradual activation of out-of-plane modes with group velocities that are roughly proportional to the wave vector.[59]

(3) Assuming isotropic boundary-scattering conditions,[60] our analysis of the layer-plane heat conductivity indicates that the phonon mean free path in turbostratic PG increases from about 600 to 1200Å as the deposition temperature covers the range 1700 to 2300°C. These mean free paths are 3 to 5 times larger than the average crystallite diameter and are believed to be indicative of the size of the polygonal zones that assemble into "wrinkled sheets"; moreover, they seem to correlate closely with the degree of preferred orientation. In this connection we should point out that thermal conductivity data taken in the lowest temperature range generate straight K_{II}/T versus $T^{3/2}$ characteristics whose slopes provide a sensitive means of assessing the texture of PG deposits.

Regarding electronic contributions to the thermal conductivity along PG layer planes the discussion in Sec. V leads us to conclude that, in both magnitude and deposition-temperature dependence, they are compatible with a simple two-band (STB) model description of the graphite band structure. This *phenomenological* model, however, is inadequate to explain all the features of electronic transport in turbostratic graphite; temperature-independent resistivity characteristics, for instance, are felt to require some overlap of the valence and the conduction band. Considering the present state of uncertainty, it may not be wise to assign much quantitative significance to STB-type calculations. Nevertheless,

(1) There is strong evidence for bipolar contributions to the electronic thermal conductivity of turbostratic PG. This phenomenon results from simultaneous conduction in the two bands, under conditions typical of a "true" Fermi-Dirac regime ($-2 \leqslant \Delta/kT \leqslant 6$). In view of the relatively large crystallite size, it is possible that the depression of the Fermi level (measured from the edge of the valence band) would not exceed a few kT even at the lowest temperatures.

(2) The Lorenz numbers derived from Eq. (20) on the assumption of an energy-independent relaxation mechanism describe the situation remarkably well. While (20) is not likely to be exact, it does show how $\mathfrak{L}$ depends on the reduced Fermi energy, and thus demonstrates that Lorenz numbers such as those listed in Table IV warrant serious consideration. Because of the semimetallic character of graphite they can be appreciably larger than the usual $\mathfrak{L}_0 = 2.45 \times 10^{-8}$ (V/°K)^2 of completely degenerate systems.

(3) As deduced from K_{II}/T intercepts, the variation of K_E with deposition temperature reflects the pattern exhibited by other electron-transport properties. It must be said, however, that the intercept technique may not be a satisfactory method of extracting the electronic thermal component in graphite. Careful magnetothermal conductivity experiments would be of great help, but it is doubtful whether these will be available in the foreseeable future, at least for turbostratic material.[53]

[58] The slightly weaker temperature dependence above 10°K reflects the truncation of "vertical" cigar-shaped constant-frequency ellipsoids associated with in-plane vibrational branches.

[59] Owing to the anisotropy of graphite crystals the over-all thermal conduction of conventional material is mainly determined by the basal-plane behavior; the approach followed here may, therefore, provide a *natural* explanation for the temperature-dependence anomaly of most graphites.

[60] The results of calculations of a phonon mean free path taken as $l(\theta) = l_a[1+(l_a^2/l_c^2-1)\cos^2\theta]^{-1/2}$, with $l_a/l_c = 2$ and 4, were presented at the 1963 March meeting of The American Physical Society; because of the averaging procedure, anisotropy in the scattering-path configuration does not critically affect the conclusions of the analysis offered in this paper.

ACKNOWLEDGMENTS

We are very grateful to Dr. J. Pappis, of Raytheon's Advanced Materials Department, and to Dr. D. Schiff, of High Temperature Materials, Inc., for providing the excellent specimens which made this investigation possible. We express our sincere appreciation to N. Albertinetti for his cooperation in taking data, and to S. Cvikevich, who contributed the x-ray diffraction results. Finally, it is a pleasure to acknowledge helpful suggestions and criticism from Professor J. Krumhansl, and to thank Dr. G. Slack for a number of comments and discussions.

APPENDIX

1. *Mean effective velocity of in-plane modes in the direction of the hexagonal axis:*

$$\langle v_{1,2}\rangle_c=\int_0^{\pi/2} v_{1,2}\cos^2\theta\sin\theta d\theta$$

$$=\int_0^{\pi/2}(v_{t,l}^2\sin^2\theta+\zeta\cos^2\theta)^{1/2}\cos^2\theta\sin\theta d\theta. \quad \text{(A1)}$$

After substituting x for $\cos\theta$, one has

$$\langle v_{1,2}\rangle_c=\int_0^1[v_{t,l}^2-(v_{t,l}^2-\zeta)x^2]^{1/2}x^2dx, \quad \text{(A2)}$$

and since $\zeta\ll v_{t,l}^2$ (see Table II), it follows that

$$\langle v_{1,2}\rangle_c=v_{t,l}\int_0^1(1-x^2)^{1/2}x^2dx$$

$$=(\pi/16)v_{t,l}. \quad \text{(A3)}$$

2. *Mean effective velocity of out-of-plane modes in the direction of the hexagonal axis (long-wavelength approximation):*

$$\langle v_3\rangle_c=\int_0^{\pi/2} v_3\cos^2\theta\sin\theta d\theta$$

$$=\int_0^{\pi/2}[\zeta\sin^2\theta+(\mu c_0)^2\cos^2\theta]^{1/2}\cos^2\theta\sin\theta d\theta. \quad \text{(A4)}$$

After substituting x for $\cos\theta$, one has

$$\langle v_3\rangle_c=\int_0^1[\zeta+(\mu^2c_0^2-\zeta)x^2]^{1/2}x^2dx, \quad \text{(A5)}$$

and since $\zeta\ll(\mu c_0)^2$ (see Table II), it follows that

$$\langle v_3\rangle_c=\mu c_0\int_0^1[\zeta/(\mu c_0)^2+x^2]^{1/2}x^2dx$$

$$\approx(\mu c_0/4)[1+\zeta/(\mu c_0)^2]. \quad \text{(A6)}$$

3. *Mean effective velocity of in-plane modes along an arbitrary basal-plane direction:*

$$\langle v_{1,2}\rangle_a=(1/2)\int_0^{\pi/2} v_{1,2}\sin^3\theta d\theta$$

$$=(1/2)\int_0^{\pi/2}(v_{t,l}^2\sin^2\theta+\zeta\cos^2\theta)^{1/2}\sin^3\theta d\theta. \quad \text{(A7)}$$

After substituting x for $\cos\theta$, one has

$$\langle v_{1,2}\rangle_a=(1/2)\int_0^1[v_{t,l}^2-(v_{t,l}^2-\zeta)x^2]^{1/2}[1-x^2]dx, \quad \text{(A8)}$$

and since $\zeta\ll v_{t,l}^2$ (see Table II), it follows that

$$\langle v_{1,2}\rangle_a=(1/2)\left[v_{t,l}\int_0^1(1-x^2)^{1/2}dx-\langle v_{1,2}\rangle_c\right]$$

$$=(3\pi/32)v_{t,l}. \quad \text{(A9)}$$

4. *Mean effective velocity of out-of-plane modes along an arbitrary basal-plane direction (long-wavelength approximation):*

$$\langle v_3\rangle_a=(1/2)\int_0^{\pi/2} v_3\sin^3\theta d\theta$$

$$=(1/2)\int_0^{\pi/2}[\zeta\sin^2\theta+(\mu c_0)^2\cos^2\theta]^{1/2}\sin^3\theta d\theta. \quad \text{(A10)}$$

After substituting x for $\cos\theta$, one has

$$\langle v_3\rangle_a=(1/2)\int_0^1[\zeta+(\mu^2c_0^2-\zeta)x^2]^{1/2}[1-x^2]dx, \quad \text{(A11)}$$

and since $\zeta\ll(\mu c_0)^2$ (see Table II), it follows that

$$\langle v_3\rangle_a=(1/2)\left[\mu c_0\int_0^1(\zeta/\mu^2c_0^2+x^2)^{1/2}dx-\langle v_3\rangle_c\right]$$

$$\approx(\mu c_0/8)[1+(\zeta/\mu^2c_0^2)\ln(4\mu^2c_0^2/\zeta)]. \quad \text{(A12)}$$